AGU PUBLICATIONS

Water Resources Research

RESEARCH ARTICLE
10.1002/2015WR017161

Landscape reorganization under changing climatic forcing: Results from an experimental landscape

Arvind Singh[1], Liam Reinhardt[2], and Efi Foufoula-Georgiou[3]

[1]Department of Civil, Environmental and Construction Engineering, University of Central Florida, Orlando, Florida, USA, [2]Geography, College of Life and Environmental Sciences, University of Exeter, Penryn, Cornwall, UK, [3]Department Civil, Environmental and Geo-Engineering, St. Anthony Falls Laboratory and National Center for Earth-Surface Dynamics, University of Minnesota, Minneapolis, Minnesota, USA

Key Points:
- Climate shifts reorganize landscapes at all scales
- Fluvial regime expands to smaller scales under increased precipitation
- Landscape reorganization mainly driven by hillslope erosion

Correspondence to:
A. Singh,
arvind.singh@ucf.edu

Citation:
Singh, A., L. Reinhardt, and E. Foufoula-Georgiou (2015), Landscape reorganization under changing climatic forcing: Results from an experimental landscape, *Water Resour. Res.*, *51*, 4320–4337, doi:10.1002/2015WR017161.

Received 28 FEB 2015
Accepted 16 MAY 2015
Accepted article online 20 MAY 2015
Published online 18 JUN 2015

Abstract Understanding how landscapes respond to climate dynamics in terms of macroscale (average topographic features) and microscale (landform reorganization) is of interest both for deciphering past climates from today's landscapes and for predicting future landscapes in view of recent climatic trends. Although several studies have addressed macro-scale response, only a few have focused on quantifying smaller-scale basin reorganization. To that goal, a series of controlled laboratory experiments were conducted where a self-organized complete drainage network emerged under constant precipitation and uplift dynamics. Once steady state was achieved, the landscape was subjected to a fivefold increase in precipitation (transient state). Throughout the evolution, high-resolution spatiotemporal topographic data in the form of digital elevation models were collected. The steady state landscape was shown to possess three distinct geomorphic regimes (unchannelized hillslopes, debris-dominated channels, and fluvially dominated channels). During transient state, landscape reorganization was observed to be driven by hillslopes via accelerated erosion, ridge lowering, channel widening, and reduction of basin relief as opposed to channel base-level reduction. Quantitative metrics on which these conclusions were based included slope-area curve, correlation analysis of spatial and temporal elevation increments, and wavelet spectral analysis of the evolving landscapes. Our results highlight that landscape reorganization in response to increased precipitation seems to follow "an arrow of scale": major elevation change initiates at the hillslope scale driving erosional regime change at intermediate scales and further cascading to geomorphic changes at the channel scale as time evolves.

1. Introduction

An extensive body of research has been devoted to understanding the effect of climate change, and more specifically changing precipitation on landscape evolution [e.g., *Smith*, 1982; *Knox*, 1983; *Bull*, 1991; *Willgoose et al.*, 1991; *Willgoose*, 1994; *Rinaldo et al.*, 1995; *Tucker and Slingerland*, 1997; *Molnar*, 2001; *Montgomery et al.*, 2001; *Milly et al.*, 2002; *Bonnet and Crave*, 2003; *Gabet et al.*, 2004; *Bookhagen et al.*, 2005; *Zaprowski et al.*, 2005; *Intergovernmental Panel on Climate Change*, 2007; *Fuller et al.*, 2009; *Godard et al.*, 2013; *Slater and Singer*, 2013]. Understanding and quantifying the effect of change in climate, in terms of changing patterns in frequency and magnitude of precipitation, on landscape evolution is important not only for predicting the impact of future climate change on landscapes but also for deciphering the signature of past climates from existing landscapes and strata [*Brakenridge*, 1980; *Smith*, 1982; *Meyer et al.*, 1992; *Tucker and Slingerland*, 1997; *Paola et al.*, 2009; *Jerolmack and Paola*, 2010; *National Research Council*, 2010; *Reinhardt et al.*, 2010; *Foreman et al.*, 2012].

In the broadest sense, an increase/decrease in long-term average precipitation is expected to decrease/increase the mean topographic elevation of a landscape [e.g., *Willgoose et al.*, 1991; *Tucker and Bras*, 1998; *Whipple et al.*, 1999; *Bonnet and Crave*, 2003]. The generally expressed view is that these topographic changes are driven by river channel incision or aggradation which in turn drives a hillslope response, i.e., rivers respond and hillslopes follow [*Whipple and Tucker*, 1999; *Dietrich et al.*, 2003; *Whittaker*, 2012]. Thus, most numerical studies have focused on the changing rates of channel erosion (typically by increasing the erosivity coefficient K in the stream-power relation $E=KA^mS^n$, where E, A, and S denote the erosion rate,

upstream drainage area, and channel slope, respectively; *K*, *m*, and *n* are the constants) [*Tucker and Slingerland*, 1997; *Tucker and Hancock*, 2010; *Lague*, 2014].

Field studies have similarly focused on channel response to precipitation change. For example, *Hartshorn et al*. [2002] argued that valley lowering is driven by frequent, moderate intensity floods which mobilize the coarse bed load and abrade underlying bedrock while *D'Arcy and Whittaker* [2014] found that channel steepness is significantly suppressed by higher precipitation due to a concomitant increase in stream power. Hillslopes are then expected to passively follow decreased or increased rates of base-level lowering by either (a) steepening or lowering hillslope angle: in transport-limited (soil mantled) conditions, the rate of soil creep/mass movement will slowly change due to a change in base level and increased/decreased soil diffusivity [*Fernandes and Dietrich*, 1997]; or (b) in high-relief terrain maintain roughly linear (threshold) hillslopes but increase/decrease the rate of landsliding [*Burbank et al*., 1996; *Tucker and Bras*, 1998; *Tucker and Hancock*, 2010]. Crucially, *Gabet et al*. [2004] while agreeing with the view that mean topographic elevation lowers in response to increased precipitation also found that relief is inversely related to precipitation. This latter finding has important implications: rather than channel incision or a change in drainage density driving hillslope lowering, gross elevation may instead be changed by a lowering of hillslope angle; or put another way hillslopes do not necessarily respond passively to base-level change as described above. Instead, by controlling the sediment supply to adjacent channels, hillslope processes directly influence channel dynamics, i.e., hillslope processes may respond to changing precipitation by either increasing or decreasing the sediment supply to adjacent channels which either enhances or impedes fluvial wear of the channel. Thus, both hillslopes and channels respond independently and interdependently [*Brunsden and Thornes*, 1979; *Brunsden*, 1993; *Sklar and Dietrich*, 1998; *Hartshorn et al*., 2002; *Dietrich et al*., 2003; *Turowski et al*., 2013; *Finnegan et al*., 2014; *Michaelides and Singer*, 2014] to changing precipitation and it is far from clear which leads the response or whether indeed their coupling means that they respond simultaneously.

Physical experiments offer a powerful means for understanding landscape evolution and for testing hypotheses under controlled settings [e.g., *Parker*, 1977; *Schumm et al*., 1987; *Hancock*, 1997; *Hancock and Willgoose*, 2001a; *Bonnet*, 2009; *Reinhardt and Ellis*, 2015]. The recent work of *Hasbargen and Paola* [2000] and *Bonnet and Crave* [2003] have shed new light on understanding the erosional variability and landscape dynamics under climatic and tectonic forcing. For instance, *Hasbargen and Paola* [2000] noticed that the long-term behavior of landscapes even under steady state and subject to steady forcing results in a highly dynamic topography (dynamic steady state), contrary to earlier numerical modeling results that lead to static landscapes. More recent numerical modeling has shown that dynamic steady states can be reproduced in models by accounting for dynamically interacting ridge-hillslope and channel processes [*Goren et al*., 2014].

In this paper, we use physical modeling to explore in detail (subbasin scale) topographic adjustments to a fivefold increase in precipitation. Although both experimental and numerical studies have increased our knowledge on the behavior of landscape erosional dynamics and their nonlinear response to change, most of these studies are largely restricted to comparison in terms of the large-scale or average change statistics, i.e., change in the mean elevation, relief, main stream profile, and stream order. To the best of our knowledge, no previous physical experiments have quantified the effect of changing climatic forcing on microscale topographical features. Such studies require very high-resolution spatiotemporal data of the elevation field which was up until now impossible to obtain. Here we present the results from a physical landscape evolution experiment performed under a controlled laboratory setting with the external forcings as constant uplift rate and time-varying precipitation rate. The goal of this study is to understand how changing precipitation patterns may influence landscape evolution by reorganizing the geometry of a landscape (e.g., subbasin boundaries, channel base level, channel networks, and hillslopes). The main hypothesis put forward is that the landscape reorganizes in a scale-dependent manner, with small scales forcing and leading the geometric adjustments of larger scales. We test this hypothesis by extensive analysis of the landscape at the steady and transient states in terms of the geometric, probabilistic, and energy redistribution of the erosional and depositional events over a range of scales.

The paper is structured as follows. In section 2, we briefly review the experimental setup, the data collected, and why physical models are analogous to natural landscapes. Section 3 is devoted to the landscape characterization at steady state in terms of its slope-area relationship and the probability of exceedance of

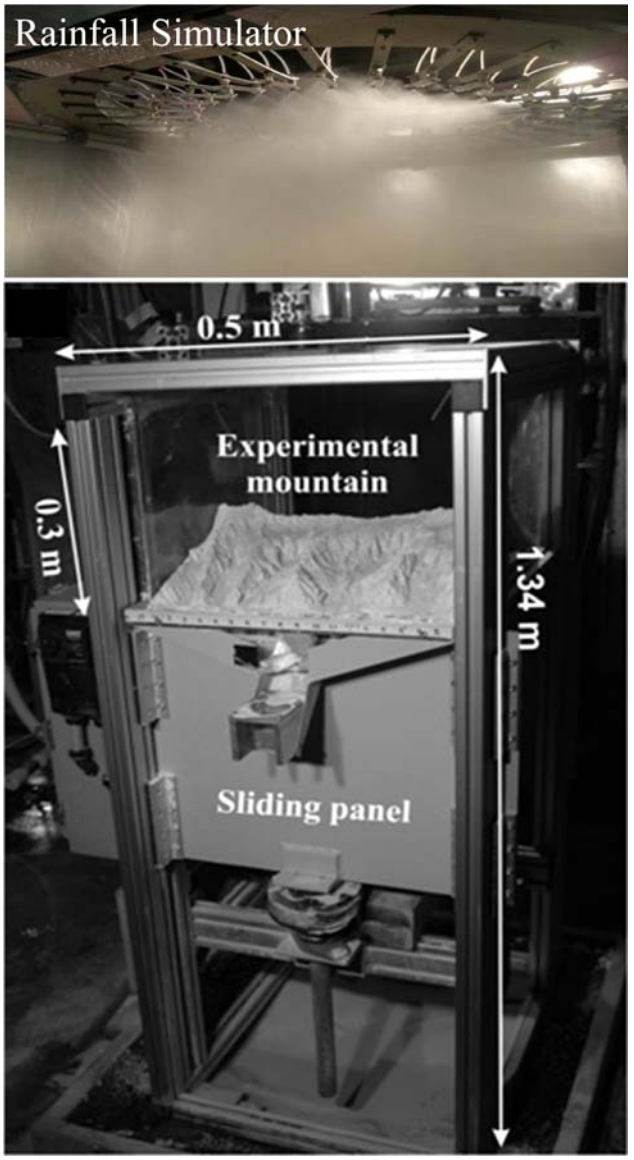

Figure 1. eXperimental Landscape Evolution (XLE) facility at the St. Anthony Falls Laboratory, University of Minnesota.

upstream contributing area, documenting in both cases the presence of power law relationships within a range of scales as observed in real landscapes. Section 4 analyzes the landscape reorganization during the transient state in terms of the changing slope-area relationship, the probability distribution function (PDF) of elevation changes (erosional and depositional events) and their spatial patterns. In section 5, we further investigate the landscape reorganization by focusing on a specific spatial transect in which elevation changes at steady and transient states are examined via a linear analysis in the space and frequency domain (autocorrelation function and power spectra) and also by local attribution of these changes. Finally, the summary and conclusions are presented in section 6.

2. Description of the eXperimental Landscape Evolution (XLE) Facility

2.1. Experimental Design and Data Collected

The experiment reported here was conducted in the eXperimental Landscape Evolution (XLE) facility at the St. Anthony Falls Laboratory at the University of Minnesota. The experimental setup included a 0.5 m $\times$ 0.5 m $\times$ 0.3 m erosion box in which two opposing or flanking sides can slide up and down at variable rates mimicking a rising or falling base level (Figure 1). Rainfall was simulated using 20 ultrafine misting nozzles (rain droplet size $<$ 10 μm) mounted over the erosion box. A variable rainfall pattern, with rain drop size small enough to avoid splash dispersion by rain drop impact on the model surface, can be produced using this rainfall simulator. However, in this study, we focus on a landscape evolved under a spatially uniform rainfall pattern. Prior to the inception of uplift, small pans were placed on the platform of the erosion basin to collect the rainfall for varying lengths of time (from 5 to 20 min). The obtained average coefficient of variation of the spatial precipitation rates was less than 5% confirming the conditions of spatial uniformity. The experiment began with an initial flat surface upon which rainfall fell and a constant uplift rate was applied.

The sediment (erodible material) used as the model substrate consisted of a homogeneous mixture of fine silica (density $\sim$ 2.65 g/cm^3), characterized by a grain size distribution (GSD) of $D_{25} = 10$ μm, $D_{50} = 25$ μm, and $D_{75} = 45$ μm, with approximately 35% water by volume mixed in a cement mixer. This mixture was achieved after laborious testing of other alternatives; silica requires severe precautions in handling to meet health standards but it was the only mixture that allowed channel formation in such a small-scale experimental setting [see also *Hasbargen and Paola*, 2000; *Lague et al.*, 2003; *Bonnet and Crave*, 2006; *Reinhardt*

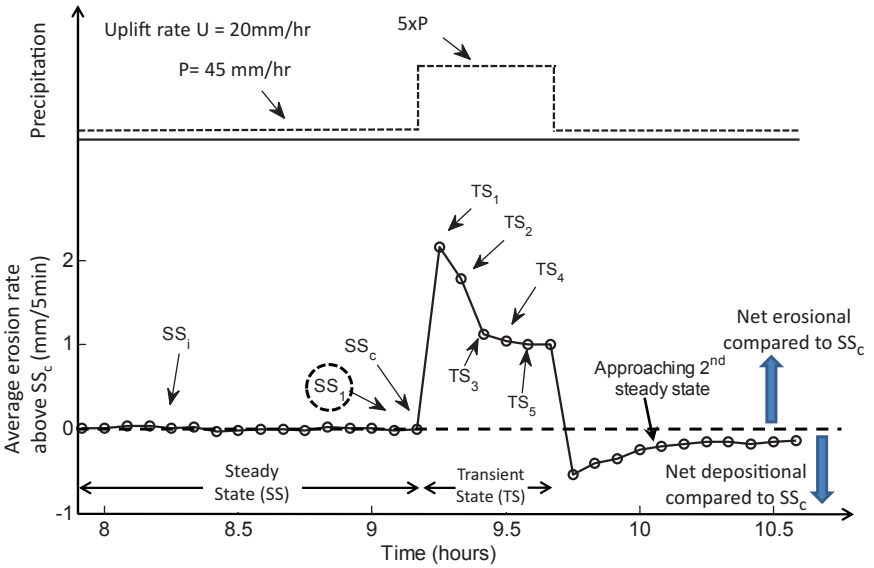

Figure 2. (bottom) Average erosion rate above that at steady state SS_c as a function of time and (top) the schematic of precipitation structure applied to the evolving landscape. Uplift rate was kept constant throughout the experiment. Precipitation (*P*) was increased to 5 times once the landscape achieved steady state (dynamic equilibrium). Steady state was accessed when sediment discharge of the landscape did not change significantly with time. *SS* denotes steady state, *TS* denotes transient state, and their subscripts (*i*, *c*, and 1–5) denote different instants of time, all 5 min apart. Subscript *c* in SS_c denotes the time instant when increased precipitation was introduced, whereas subscript *i* denotes time instants at steady state *SS*. The full probability distribution of the pixel-wise erosional and depositional values between elevations at steady state ($SS_1 - SS_c$) and transient state ($SS_c - TS_1$) is shown in Figure 6.

and Ellis, 2015]. The mixed material was allowed to settle in the basin for approximately 24 h. The resulting model substrate was flat and impermeable leading to no groundwater flow. We note that, although permeability variations and subsurface flow are important components of most natural environments, here these aspects are absent and changes in landscape reorganization are only attributable to changes in rainfall rates (see section 2.2 for more discussion).

The experimental setup also included an advanced laser scanner which can scan the whole model surface within a few seconds at a very high resolution both in space and time; the laser scanner takes ~4 s to scan a surface of area 0.5 m × 0.5 m at a resolution of 0.5 mm. However, the total time between stopping and restarting the rain for data collection was ~55 s, which was sufficient to drain water through the evolved drainage network resulting in a dried topographic surface for the laser scan. The vertical accuracy of the laser scanner depended on the distance from the laser camera to the model surface and in this experiment it was less than 0.5 mm. Note that this estimate of the vertical accuracy is a highly conservative estimate of the actual vertical accuracy materialized in our experiment.

With the initiation of the experiment, the two flanking sides moved downward creating relief on each edge of the basin, which in return developed erosional instabilities, under the combined action of uplift and rainfall that propagated upstream into the initially flat surface. These instabilities (initially in the form of rills, almost equally spaced) further developed into channels, formed knick points, and moved upward by incising into the basin until the landscape was completely dissected and the main drainage divide (MDD) was formed. Once the MDD was formed, the landscape achieved a statistical steady state for a given uplift and rainfall rate. Here we define steady state (*SS*) as the state of the landscape at which the mean elevation (or mean erosion rate) of the evolved landscape does not change with time. In other words, at *SS*, the mean erosion rate completely balances the uplift rate [*Hack*, 1960].

Figure 2 shows the average erosion rate above SS_c (i.e., obtained by removing the mean erosion rate at steady state SS_c) over the landscape as a function of time and the schematic of the precipitation structure applied to the landscape (see caption of Figure 2 for definition of different states and their subscripts). *SS* was achieved for a spatially uniform and constant rainfall rate P = 45 mm/h and a constant uplift rate U = 20 mm/h. During *SS*, a perturbation was introduced with the precipitation rate increased by a factor of 5 for 30 min (see Figure 2). The experiment was terminated once the flanking sides reached the bottom of

the erosion box, i.e., ~30 cm of base-level fall, which was approximately 15 h after initiation of the run. High-resolution digital elevation models (DEMs), with a 0.5 mm grid size, of the entire basin were collected every 5 min during the experiment. In addition, still photographs over the whole experimental basin were also captured every 5 min.

2.2. Scaling and Realism of the Experiment

Steady state landscapes are essentially timeless (i.e., the mean statistical properties of the landscape do not change through time) [*Hack*, 1960], thus the time scale relevant to this research is the time over which we simulated a climatic perturbation. Using a scaling argument, this transient time was converted to real time as $T_{real} = \frac{R_{real} \times T_{exp}}{U_{real} \times T^e_{exp}}$; for example, 1 min in our experiment corresponds to approximately 100 years in a natural system assuming an average uplift rate U_{real} and average relief R_{real} of a mountain are 1 cm/yr and 500 m, respectively. Here T_{exp} is the experimental time, whereas T^e_{exp} is the experimental equilibrium time, i.e., the time at which the landscape achieves steady state which is approximately 8 h in our experiment (see time axis in Figure 2). Thus, to a gross approximation, our experiment represents an equilibrium state and the perturbation of increased precipitation (which lasted for 30 min translated to 3000 years in our experiment) is interpreted as a climatic trend, i.e., a shift to an increased mean annual precipitation regime of a type observed in many parts of the world over millennial time scales [e.g., *Baker et al*., 2001; *Burnett et al*., 2011]. Note that uplift rates ~ 1 cm/yr have been observed in natural landscapes [see for example, *Lavé and Avouac*, 2000; *Lague and Davy*, 2003].

We acknowledge that these physical experiments are an over simplification of natural systems as they do not account for many physical, chemical, and biological processes such as vegetation, soil heterogeneity, ground water, and soil weathering but, nevertheless, help us to gain a better understanding of how individual external forcings influence the evolution and reorganization of landscape systems.

Along these lines, we also note that the selection of fivefold increase in precipitation, which was mainly based on technical considerations (e.g., experimental basin depth and rainfall sprinklers configuration) in our experimental setting, is perceived as representing conditions where sediment supply to channels would outweigh channel streamflow increase, thus rendering the channel system transport limited. Although this condition might represent only a subset of natural settings, it is still within practical interest both in understanding landscape reorganization under extreme change in climate forcing and in learning by contrasting landscapes that have evolved under diverse climatological forcings. For example, *D'Arcy and Whittaker* [2014] studied the relation between channel steepness and precipitation rate for a large number of channels in different mountainous areas, where those mountainous regions exhibited a 10-fold range in precipitation rate but had similar uplift rates.

3. Physical Characteristics of the Evolved Landscape at Steady State

The steady state experimental landscape developed under a constant precipitation and uplift rate is shown in Figure 3. It is observed that the landscape self-organized into a pattern strikingly similar to that of real landscapes with eight drainage basins of different shapes and sizes containing fifth-order channel networks (Figure 3c). The channel networks were extracted from the DEM using the D8 algorithm [*Tarboton*, 1997] and a channel initiation threshold area of 25 mm^2 (100 pixels). The exceedance probability, characterizing drainage organization and network connectivity, of upstream contributing areas is presented in Figure 4 showing a power law of slope − 0.5 very similar to that of real landscapes [see e.g., *Rodríguez-Iturbe et al*., 1992; *Rigon et al*., 1996]. As previously noted by *Hasbargen and Paola* [2003] for experimental tributary networks and *Sapozhnikov and Foufoula-Georgiou* [1997] for experimental braided river networks, during steady state, our landscape exhibited a notable degree of internal variability (dynamic steady state) although the average basin erosion rate remained constant (see Figure 2 and also *Reinhardt and Ellis* [2015]).

The slope-area relationship is one of the most commonly used metrics to study landscape organization and its connection to the underlying physical mechanisms (such as, erosional and depositional processes) giving rise to landscape and its emergent organization at different scales [e.g., *Rinaldo et al*., 1993; *Rigon et al*., 1994; *Tucker and Bras*, 1998; *Hancock and Willgoose*, 2001a, 2001b; *Montgomery*, 2001; *Dietrich et al*., 2003; *Booth et al*., 2013]. The topographic slopes here were computed from DEM using the steepest downslope

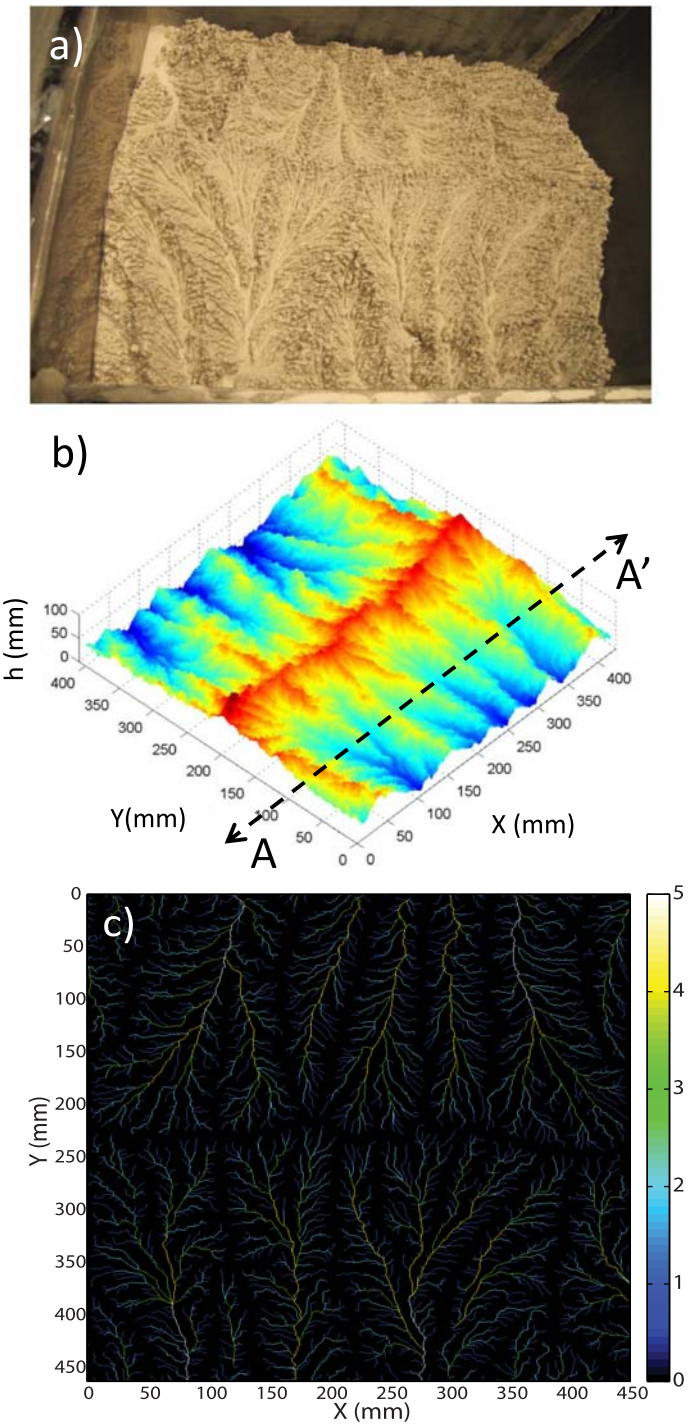

Figure 3. (a) Sample photograph and (b) the DEM of the evolved landscape at steady state (state SS_1, highlighted with dashed circle in Figure 2). AA′ on Figure 3b represents the transect used in computing spatial and temporal elevation changes (Figures 11 and 12) and the wavelet spectra (Figure 13). (c) The river network at the steady state extracted from the DEM at steady state SS_1 with the color bar indicating Strahler channel order. Notice the fifth-order channels present in the drainage basins.

direction, whereas the drainage areas were computed using the D-infinity algorithm [e.g., *Tarboton*, 1997; *Dietrich and Perron*, 2006; *Booth et al.*, 2013]. Figure 5a (open and filled black circles) shows the slope-area curve at two instants of time (5 min apart) during the *SS*. The plot is displayed in log-log scale where linearity implies a power law slope-area relationship, $S=KA^{-\theta}$. Broadly speaking, we identify three distinct regimes on that plot. At very small scales (from a single pixel size to approximately 10 pixels or 2.5 mm^2),

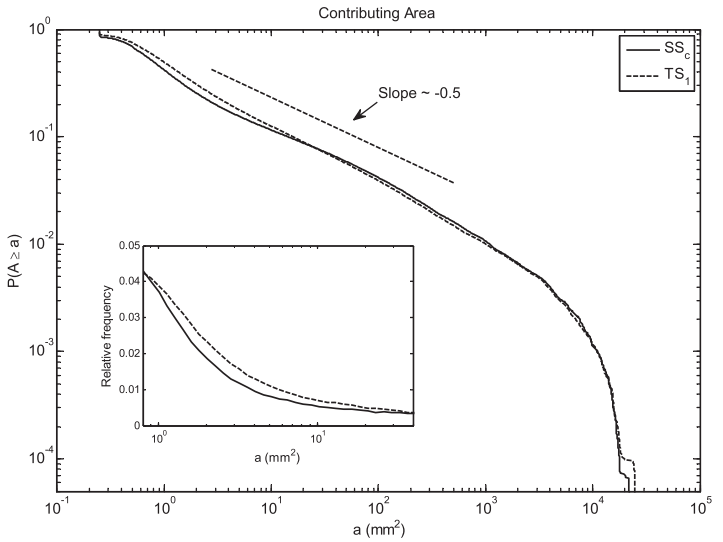

Figure 4. Exceedance probability of the contributing area (a) for the evolved landscape at steady state SS_c (solid line) and transient state TS_1 (dashed line). The power law exponent of the exceedance probability (~ -0.5) is close to that observed in real landscapes [see e.g., *Rigon et al*., 1996]. The inset figure shows the zoomed-in PDF of contributing areas 0.8–40 mm^2 corresponding to the areas of mainly first-order drainage basins, where most of the probability change occurs.

the lack of a scaling regime depicts the unchannelized parts of the landscape. The log-log linear curve at intermediate scales (drainage areas of 2.5 mm^2 to around 250 mm^2) suggests a scaling regime with a power law scaling exponent $\simeq 0.1$. This low-scaling exponent is a characteristic of colluvial type of landscapes [e.g., *Montgomery and Foufoula-Georgiou*, 1993; *Lague et al*., 2003; *Montgomery*, 2001; *Dietrich et al*., 2003; *Bonnet and Crave*, 2006] and is referred to here as the debris-dominated regime. Similar low power law exponents were observed by *Lague et al*. [2003], *Hasbargen and Paola* [2003], and *Bonnet and Crave* [2006] in their physical experiments. For larger scales ($>$250 mm^2 corresponding to approximately second-order and higher-order basins), a transition to a different power law relationship with a larger exponent (approximately 0.3) is observed, although with increased variability due to the limited data at those larger scales. We interpret this regime as a fluvially dominated regime [*Montgomery*, 2001; *Dietrich et al*., 2003]. In the next section, the evolution of the slope-area relationship as the landscape reorganizes under a fivefold precipitation increase will be discussed to gain insight into the erosional mechanisms responsible for that reorganization.

4. Response of Steady State Landscape to Climatic Forcing

4.1. Slope-Area Relationship

Figure 5a shows the slope-area relationships during the transient state (TS_1 to TS_5). Comparing these relationships with those at steady state, we observe a rapid initial reorganization of the landscape (first 5 min) followed by a slowdown in landscape response. This rapid initial reorganization is reflected in a considerable change of the shape of the slope-area relationship, with the fluvially dominated regime (slopes of approx. 0.3) shifting to smaller scales and the debris-dominated regime (slopes of approx. 0.1) shrinking and now contained within a smaller range of scales. To better illustrate this, we plot in Figure 5b the slope-area curves normalized by the power law relationship ($S^* = KA^{-\theta^*}$) with exponent $\theta^* = 0.108 \simeq 0.1$ fitted to the debris-dominated regime in *SS* (see Figure 5a). In this normalized plot, segments of log-log linearity with a slope of 0.1 display as horizontal lines. The clear shrinkage of the debris-dominated regime (shrinkage of the spatial extent of the horizontal lines) progressively replaced by the fluvially dominated regime is apparent. Most of the regime shift (from debris to fluvial) takes place at the initial 5 min where the scale of transition changes from approximately 250 mm^2 to approximately 25 mm^2 (depicted by the arrow in Figure 5b), indicating a substantial regime shift of the erosional mechanism in that range of intermediate scales (25–250 mm^2).

The probability of exceedance (in log-log scale) of the upstream contributing areas in the transient state is shown in Figure 4. Although hardly distinguishable from that at steady state, a closer examination of the

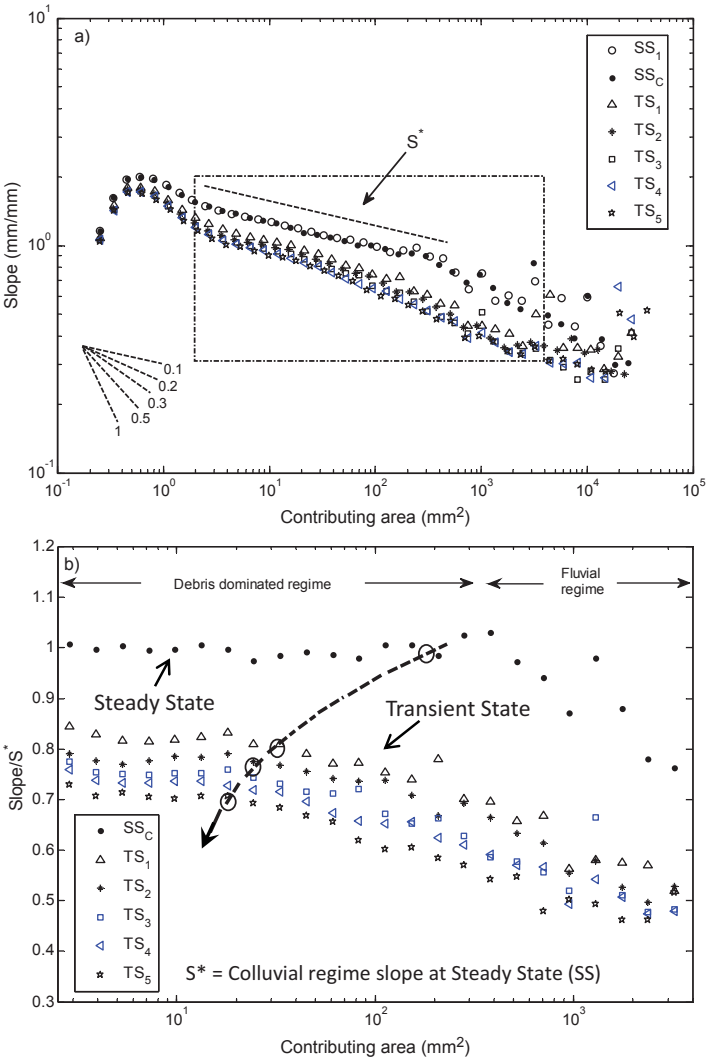

Figure 5. Fluvial regime shifts to smaller scales during *TS*. (a) Log-log plots of the slope-area curves for the self-organized landscape as it evolves from steady state (SS_1, SS_c) to transient states (TS_1 to TS_5); see Figure 2 for definition of the states. (b) Normalized and zoomed-in slope-area curve shown in Figure 5a (in the box) and for the steady and the transient states. The curves are normalized by the slope-area relationship, characterized by slope S^* ($=KA^{-\theta^*}$, where $\theta^*=0.108 \simeq 0.1$), of the landscape at the steady state SS_c. The arrow in this figure highlights that the exponent of the power law relationship increases and the scale of the onset of fluvial regime shifts toward smaller scales as the landscape adjusts to increased precipitation, whereas black circles on the arrow depict inflection points.

relative frequency plot (see inset figure) demonstrates a change in relative frequency for scales less than approximately 40 mm^2 with an increased probability of such small drainage basins (here corresponding to mostly first-order basins) at transient state. Putting this into perspective with the previously reported shrinking of the debris-dominated regime via expansion of the fluvially dominated regime within scales of 25–250 mm^2, we interpret this as the first quantitative evidence of the scale continuum of reorganization. This observation poses then the question of understanding the scale-direction of change and its mechanistic origin. In the next section, we focus on the spatial organization of elevation change via an analysis of the pixel-wise elevation differences to understand how erosional and depositional events might have redistributed over the landscape in response to the increased precipitation.

4.2. Statistics and Spatial Distribution of Elevation Changes

Figure 6 shows the PDFs of elevation differences ($\Delta h(x,y,\Delta t)=h(x,y,t)-h(x,y,t+\Delta t)$; where $\Delta t = 5$ min) between landscapes at two time instants at the steady state ($SS_1 - SS_c$) and at transient state ($SS_c - TS_1$). Positive values of $\Delta h(x,y,\Delta t)$ indicate erosion at location (x, y), while negative values indicate deposition

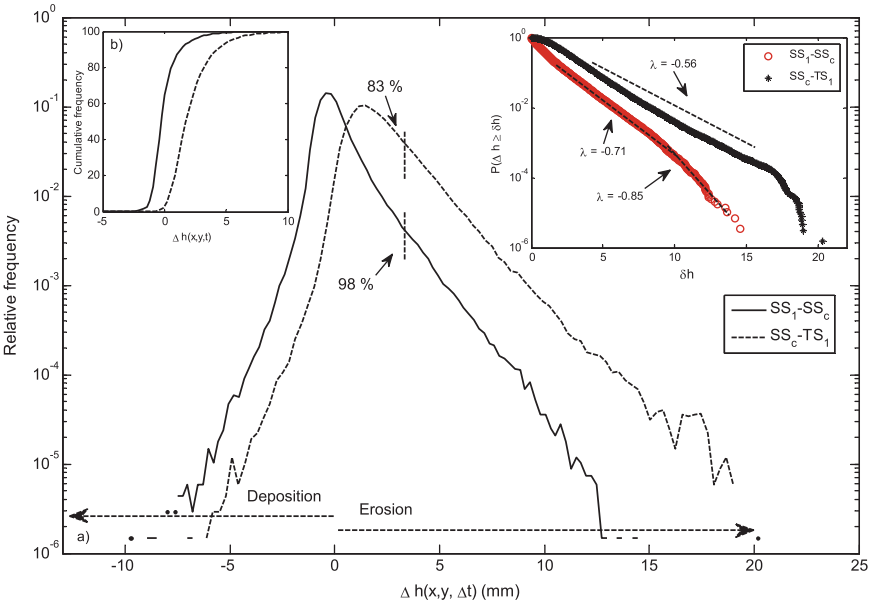

Figure 6. Higher frequency of large erosional events at *TS*. (a) PDFs and (b) the cumulative frequency distributions of the elevation differences between topographies 5 min apart during steady states ($SS_1 - SS_c$; solid line) and transient state ($SS_c - TS_1$; dashed line). Differences were computed at all pixels as $\Delta h(x, y, \Delta t) = h(x, y, t) - h(x, y, t + \Delta t)$, where $\Delta t = 5$ min. The positive $\Delta h(x, y, \Delta t)$ indicates erosion while negative $\Delta h(x, y, \Delta t)$ indicates deposition. Note the higher asymmetry in the transient state indicating higher frequency of large erosional events. Inset in Figure 6a shows the exceedance probabilities of the positive differences ($\Delta h(x, y, \Delta t) > 0$) in elevation between steady states SS_1 and SS_c (circles) and SS_c and TS_1 (asterisk). A clear slower rate of decay in the extreme values of the elevation change is observed during the *TS*. At the *SS*, a scaling break is observed at an elevation difference of ~10 mm below (>10 mm) which the exceedance probabilities decay faster. Both the regimes at the *SS* can be characterized by an exponential decay, whereas at the *TS*, a truncation from the exponential regime is observed at an elevation difference of ~17 mm. The vertical dashed lines in center of the plot represent the threshold elevation change for both *SS* (98th percentile) and *TS* (83rd percentile).

during a time interval of 5 min. Although not displayed here, it is noted that the PDFs of elevation change at different time instants during *SS* did not change and were indistinguishable from the PDF reported in Figure 6 for $SS_1 - SS_c$. The mean and the standard deviation of the elevation differences at *SS* are 0.12 and 1.15 mm, whereas at *TS* are 2.28 and 1.66 mm, respectively.

The PDFs are displayed in a semilog plot, where a straight line indicates agreement with an exponential distribution. As can be seen from this figure, the PDF at the *TS* is shifted toward the right depicting the increase in the mean net erosion rate (2.28–0.12 mm) in agreement with the results previously presented in Figure 2. In addition to the shifting of the mean, the PDF at the *TS* becomes more asymmetric to the right indicating a disproportionately higher frequency of occurrence of mid to large magnitude erosional events under *TS* compared to *SS*. Concentrating on the PDFs of erosional events ($\Delta h > 0$) only, the inset of Figure 6 shows that they are well approximated by an exponential distribution with parameter $\lambda = 0.71$ at *SS* and $\lambda = 0.56$ at *TS* further documenting (with a slow decay rate, λ, at *TS*) the disproportional increase of large erosional events in *TS*.

Considering an erosional event of magnitude ~ 3.6 mm in 5 min (mean plus three standard deviations of the PDF of Δh at *SS*) which is argued here to correspond to landslide and mass wasting type of events, Figure 7 shows the pixel-wise elevation changes exceeding that threshold, superimposed on the river network, at *SS* (Figure 7a) and *TS* (Figure 7b). Clearly, more events exceeding 3.6 mm are seen at the *TS* compared to *SS* (in fact 3.6 mm corresponds to the 98th percentile at *SS* and 83rd percentile at *TS*; see Figure 6b), but it is insightful to examine their locations and spatial extents relative to the river network. We observe that these erosional events result predominantly from the hillslopes at the *TS*. In fact, only a very few large erosional events are observed along the river paths at *TS* (see Figure 7b) in contrast to more so at *SS* (see Figure 7a). This goes against the classic landscape theory where one would expect channels to be the first responders to a climatic perturbation (by lowering their base-level elevation) and the hillslopes to follow, per discussion in section 1. We consider this as the second piece of evidence that the across-scale reorganization is not driven by channel changes but rather by changes in the unchannelized parts of the

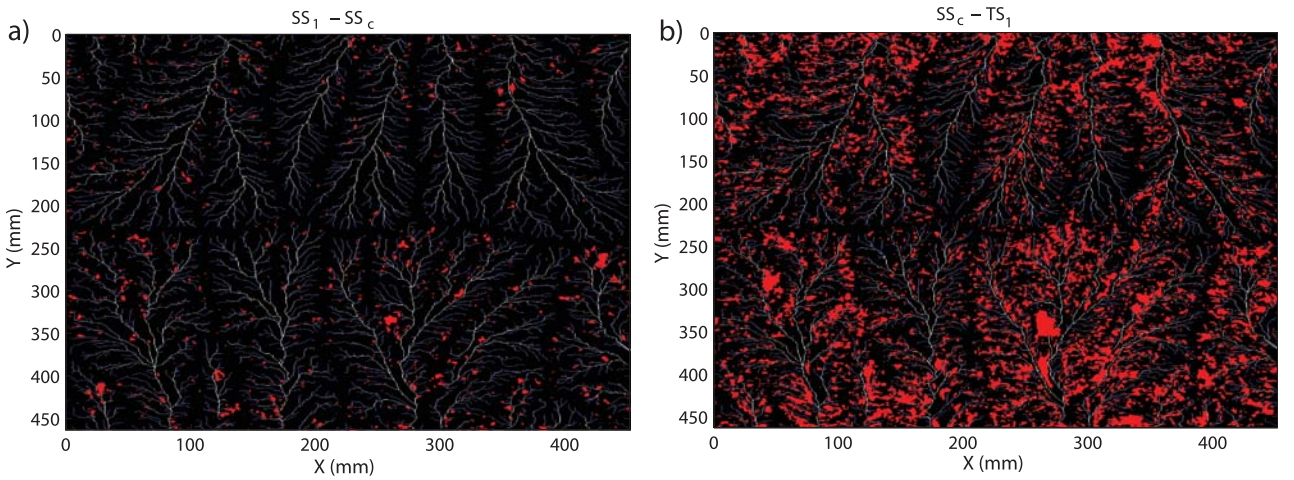

Figure 7. Spatial location of high erosional events at *SS* and *TS*. Superimposed thresholded elevation difference for $\Delta t = 5$ min on the extracted river network (Figure 3c) for (a) the steady state $SS_1 - SS_c$ and (b) the transient state $SS_c - TS_1$. The threshold elevation change is ~3.6 mm (in 5 min) which corresponds to 98th percentile in the case of *SS* and 83rd percentile in the case of *TS* (see also Figure 6). The red corresponds to erosion > 3.6 mm.

landscape. In addition, this increasing proportion of the large erosional events on the hillslopes at the *TS* further emphasizes the fact that channels are driven to fluvial state at smaller scales (see also Figure 5).

To quantitatively compare the percentage of the eroded pixels that correspond to hillslope versus channel locations under *SS* and *TS*, we perform the same analysis but by choosing the threshold not at a fixed value but at a fixed percentile, ensuring the same number of eroded pixels (representing same overall eroded area over the landscape). Here the 75th percentile was chosen which corresponds to 0.5 mm for *SS* and 3 mm for *TS*. Zooming down to a smaller area corresponding to one of the sub basins, Figures 8a and 8b show the contribution of channels and hillslopes to extreme erosion at *SS* and *TS*, respectively. Visual inspection suggests that hillslopes drive the erosional process during the transient state. This is further quantified in Figure 8c where at TS_1 only ~7% of the eroded pixels coincide with channelized pixels (percentage of channelized pixels is ~6.5% of the total landscape pixels at the SS and did not change considerably from SS_c to TS_1) compared to 13% at *SS* (tested for statistical significance using two-sided chi-square test with α=0.05), further supporting the hypothesis that hillslopes are the main contributors to erosion at *TS*. The increased erosion from nonchannelized pixels during *TS* is expected to decrease the local relief of basins. This is independently verified by looking at the PDFs of local relief (computed as the differences in elevation between every ridge pixel and adjacent channels of third order or higher) at *SS* and *TS* (Figure 9) which documents that the relative frequency of larger local relief decreases (for a range ~24–36 mm) during *TS* and is statistically significant (tested using chi-square test as mentioned above for channelized eroded pixels). Combining this with the observation that during *TS* a smaller number of channels contribute to erosion compared to *SS*, the conclusion is made that landscape reorganization is driven by hillslopes via accelerated erosion, ridge lowering, and reduction of basin relief as opposed to channel base-level reduction.

Figure 10 clearly shows that during *TS* mean slope angle progressively decreases. This is consistent with relief reduction in the local relief range discussed above (see Figure 9), as also previously observed in the field by *Gabet et al.* [2004]. During the initial transition to a much wetter climate, and given that infiltration does not occur in this experiment [see e.g., *Pelletier et al.*, 1997; *Gabet et al.*, 2004], a reduction in slope angle implies a move away from threshold dominated landsliding and toward increased erosion via Hortonian overland flow. We suggest that increased surface flow inundates minor surface irregularities to effectively increase friction [*Abrahams et al.*, 1986; *Abrahams and Parsons*, 1991] and thus shear stress such that the threshold for particle entrainment is more often exceeded. Note that once the climatic perturbation (5*P*) was over, the topography reverted back to its original state termed here as second steady state (see Figure 10 and also Figure 2); however, a small decrease in the average erosion rates, compared to *SS*, is observed in the second steady state (Figure 2). A detailed quantification of similarities and differences of the landscape at the second steady state with *SS* and *TS* will be the focus of a future study.

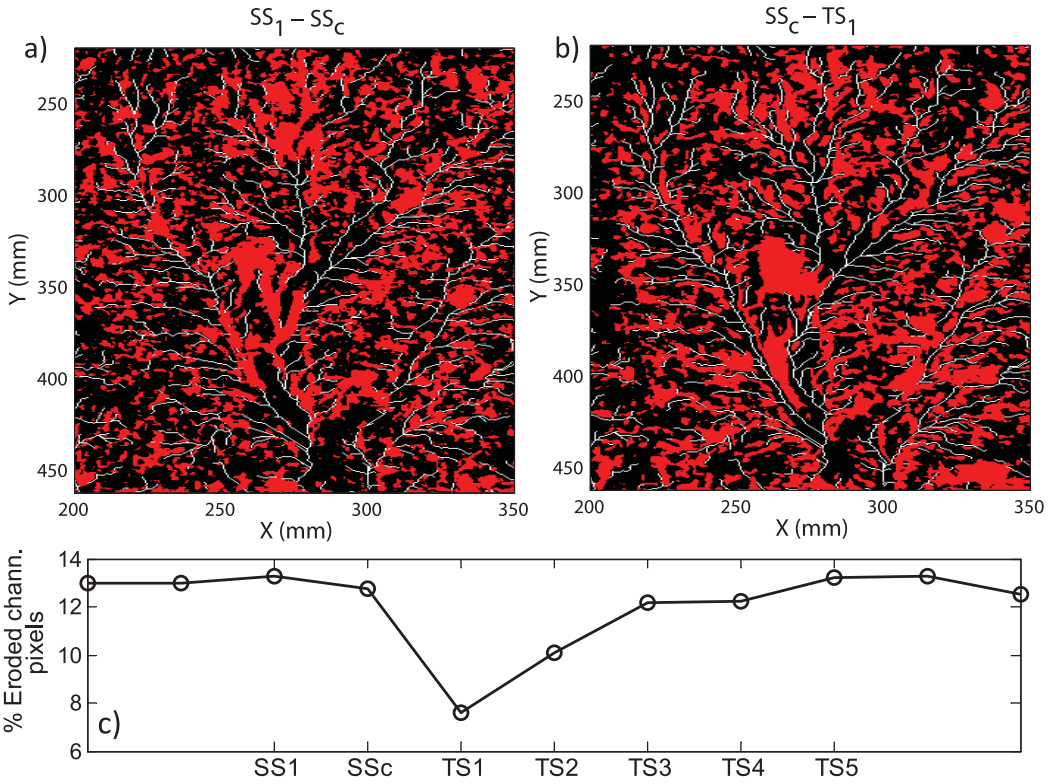

Figure 8. Regime shift in large erosional events from channel to hillslopes during the *TS*. Zoomed-in and superimposed thresholded elevation differences for $\Delta t = 5$ min on the extracted river network (Figure 3c) shown in Figure 7 for (a) the steady state $SS_1 - SS_c$ and (b) the transient state $SS_c - TS_1$. The threshold elevation difference used is the 75th percentile and corresponds to erosion events $\geq$0.5 mm in the case of *SS* and $\geq$3 mm in the case of *TS* over 5 min (see also Figure 6). Notice the significant erosion from the channels at the *SS*, whereas from the unchannelized (hillslopes) parts of the landscape at *TS*. (c) Percentage of eroded channelized pixels computed as (no. of eroded channelized pixel/total no. of channelized pixels) as a function of time.

5. Valley/Channel Widening

In the previous section, we observed that the majority of large erosional events during *TS* is from the unchannelized part of the landscape, i.e., hillslope erosion. In this section, we provide a closer quantification of the locations and scales at which erosion occurs and also look at the evolving properties of channel cross sections. For that, we focus on a transect AA′ positioned parallel and at a horizontal distance of 150 mm from the MDD (see Figure 3b). Figure 11a shows the mean-removed elevations at the spatial transect AA′ at time instants SS_1 and SS_c during steady state and at time instant TS_1 at the transient state. The SS_1 and SS_c elevation transects overlap with each other implying an inherently similar spatial structure under steady state. Conversely, we observe a significant difference in the elevation profile from state SS_c to state TS_1. This is better depicted from the series of spatial increments of these two transects: $\Delta h_x = h(x+\Delta x, y, t) - h(x, y, t)$, where $\Delta x = 0.5$ mm is the resolution of our DEMs (see Figures 12a and 12b for SS_c and TS_1, respectively).

A rougher landscape will result in a more spiky increment series (due to high variability in adjacent elevations) while a smoother landscape will result in an increment series with reduced spikes and larger uninterrupted regions of same-sign increment values (depicting smoothly increasing or decreasing elevation of valleys and hillslopes). Figure 12b clearly demonstrates the landscape smoothing at TS_1 (see highlighted areas by ellipse as well as locations A, B, and C in Figure 11a and its inset plots A and B). This smoothing is further documented in the autocorrelation function (ACF) of spatial increments which shows the elimination of distinct scales of approximately 4 and 8 mm present at SS_c and an increased autocorrelation within scales 2–10 mm at TS_1 (Figure 12c). This provides the third piece of evidence of the reorganization of the unchannelized parts of the landscape at transient state.

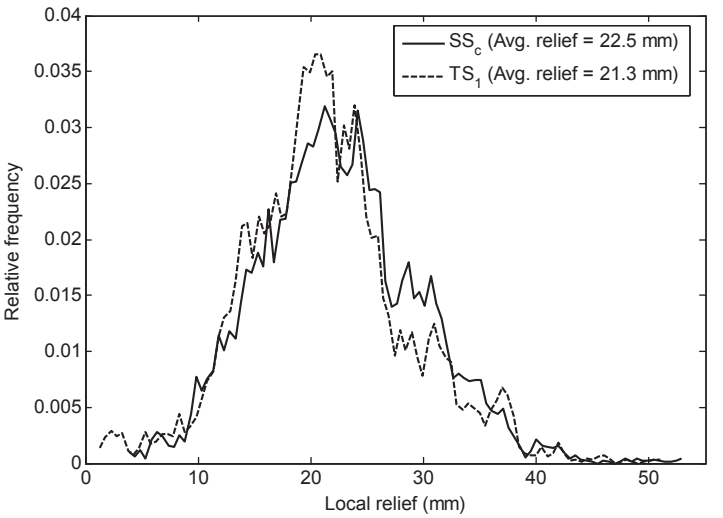

Figure 9. Decreased frequency of larger magnitude local relief at *TS*. Local relief (defined as the elevation difference between each ridge pixel and the adjacent channel floor) of the evolved landscape at steady (SS_c) and transient (TS_1) states. The decrease in the relative frequency of larger relief at the transient state is in agreement with the lowering of ridges in small to intermediate size basins due to landscape smoothening at those scales and is consistent with the replacement of a debris-dominated regime with a fluvially dominated regime (Figure 5).

While the structure of spatial increments at SS_c and TS_1 depicts the smoothness (or lack of) in the landscape at a frozen state, the temporal elevation differences (from SS_1 to SS_c and SS_c to TS_1) depict more directly the time-evolving landscape. It is expected that the $SS_c - TS_1$ temporal elevation differences will have a larger mean and a larger variance compared to those from $SS_1 - SS_c$ and this is clearly observed in Figure 11b. Although the spatial arrangement of these temporal elevation changes is hard to evaluate visually, they are clearly depicted in the ACF (shown as the inset). We observe an increased spatial autocorrelation of the ($SS_c - TS_1$) series quantifying once more the spatial coherence of the temporal elevation changes during the transient state. In addition, the ACF reveals an emergent increase of spatial correlation at scales of approximately 10–15 mm in agreement once more with the emergence of intermediate to large-scale structures (100–200 mm^2) during the transient state from erosional changes in the much smaller-scale unchannelized (hillslope) parts of the landscape.

Increased surface runoff and hillslope erosion leads to channel widening and, under transport-limited conditions, to channel and valley aggradation (see locations E, F, G, H, and K in Figure 11a and the inset plots F, G, and H). To quantitatively measure the widening of channels and valleys observed in Figure 11a and its insets, we identified ~230 channels obtained from 26 different transects at SS_c and TS_1 intersecting channels of fourth order and fifth order and computed the channel cross-sectional statistics. The results suggest that on average, at the *TS*, the channels widened by a factor of ~ 1.4 times the channel width at SS_c. In view of the observed channel widening along with the relative decrease in channel erosion (as documented in the above sections), we conclude that river bed elevation does not lower but rather remains stable or aggrades, suggesting hillslope erosion is the main driver of the landscape reorganization, although channel-hillslope coupling is maintained.

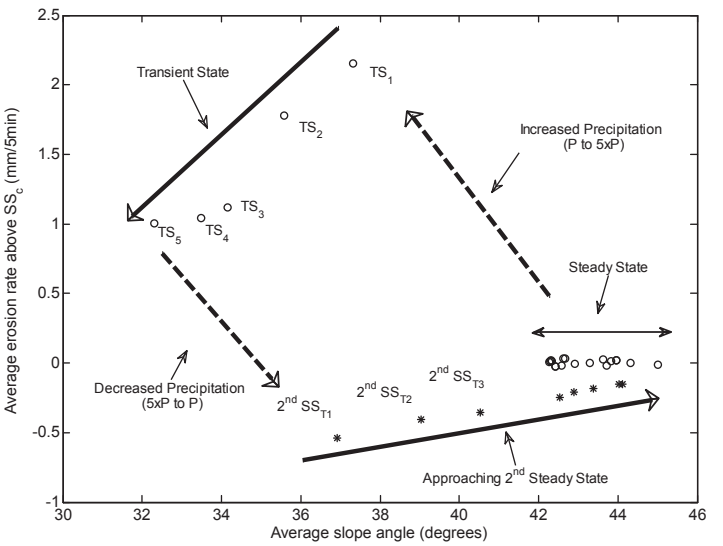

Figure 10. Average erosion rate above SS_c (see Figure 2) as a function of the average slope angle (computed as the average of the local slopes used in the slope-area curve) and time for both steady and transient states. Solid circles represent steady (*SS*) and transient (*TS*) states, whereas asterisks represent landscape at different times after *TS* approaching second steady state.

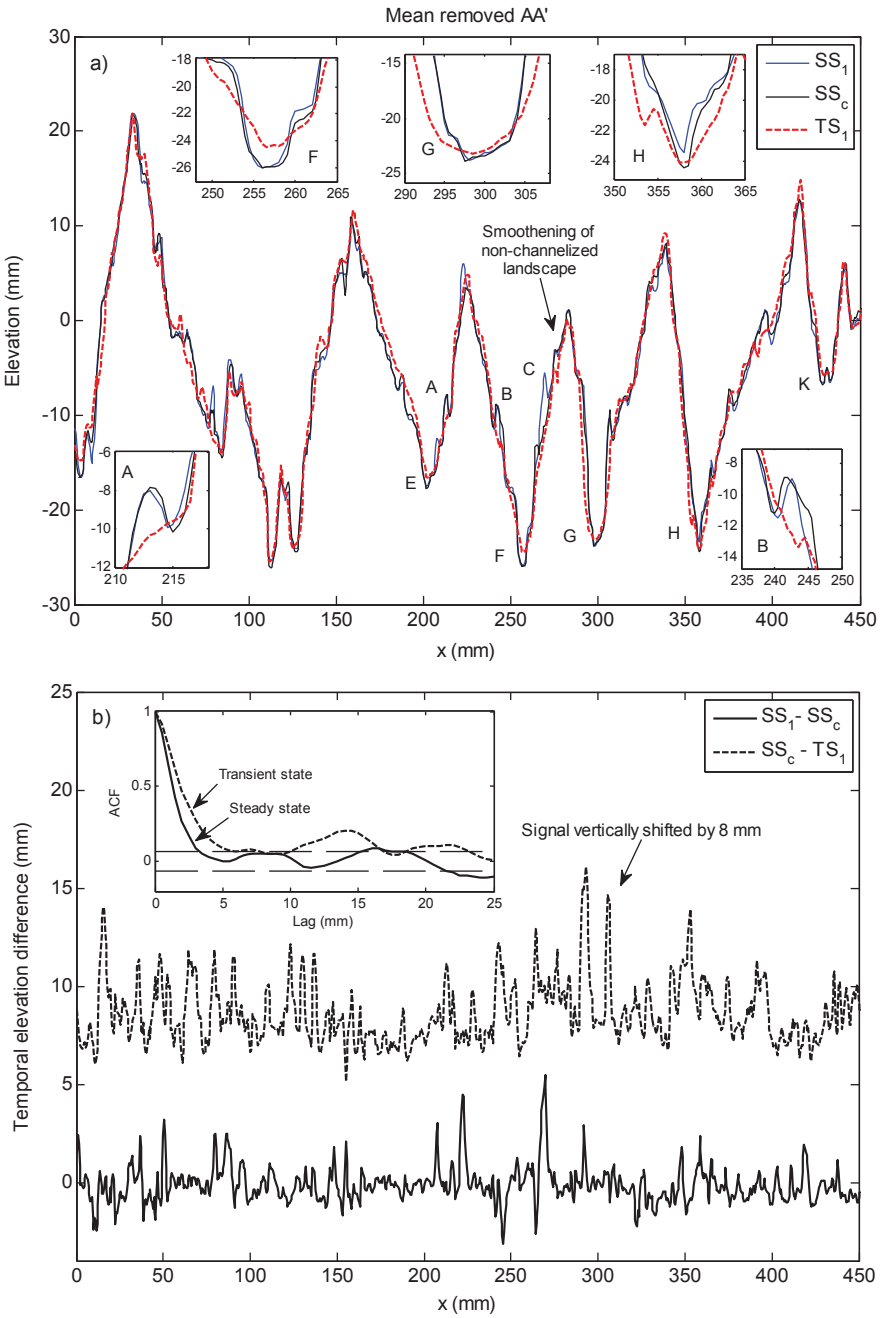

Figure 11. Channel widening and hillslope smoothening during *TS* as documented by the temporal evolution of an elevation transect. (a) Transects AA′ (shown in Figure 3b) for the two steady states SS_1 and SS_c and the transient state TS_1. Notice that at the steady states, the structure of the transects is very similar and overlapping. Insets in this figure show zoomed-in channelized locations marked as F, G and H on the transects illustrating the widening of channels at *TS* (this has been confirmed by an analysis of 230 individual channel cross sections; see text) along with zoomed-in locations of smoothed hillslopes marked as A and B. (b) Temporal elevation differences at steady state ($SS_1 - SS_c$) and transient state ($SS_c - TS_1$) of transect AA′, whereas the inset figure shows their autocorrelation functions (ACFs). Elevation differences at transient state ($SS_c - TS_1$) are vertically shifted by 8 mm for display purpose. The horizontal dashed lines in the inset figure show the 95% confidence level limits.

The power spectral density (PSD) is an effective way of quantifying how the variance of a process is distributed across scales and has been extensively used for characterization of landscapes [e.g., *Pelletier*, 1999; *Passalacqua et al.*, 2006; *Perron et al.*, 2008; *Singh et al.*, 2010; *Guala et al.*, 2014; *Keylock et al.*, 2014]. From the PSD of spatial elevation increments at transect AA′ at SS_c (Figure 13), three distinct scaling regimes are observed. At the lower wave numbers (larger wavelengths $\sim$ 7–2.5 cm), the scaling regime shows a power

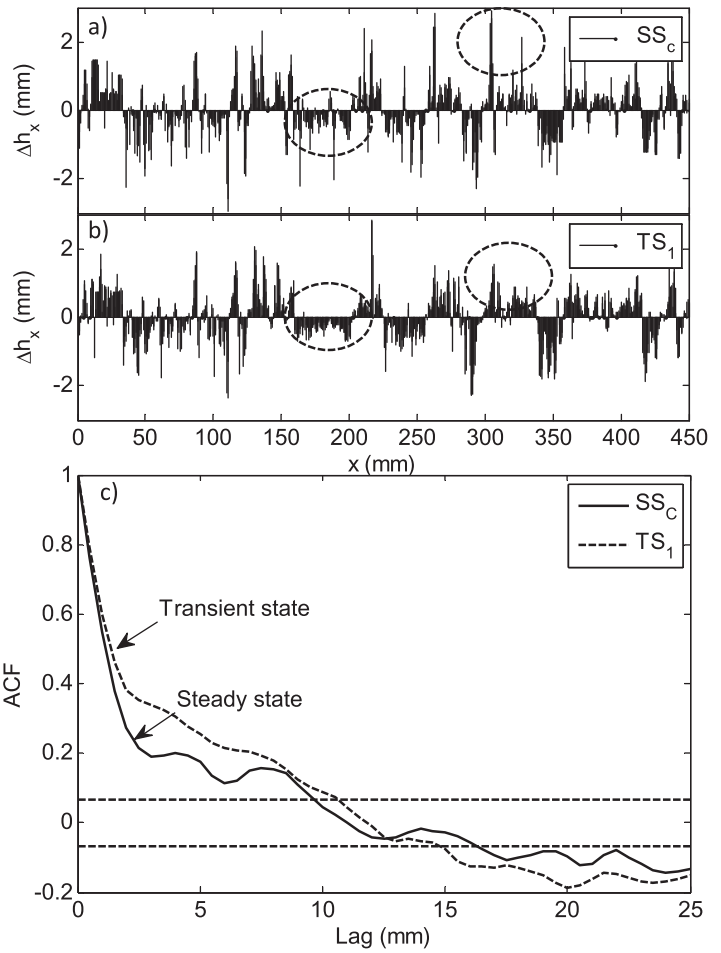

Figure 12. Smoother hillslopes at *TS* as documented by the less spiky and more autocorrelated nature of adjacent pixel elevations at an elevation transect. Spatial elevation increments ($\Delta h_x = h(x,y,t) - h(x+\Delta x, y, t)$) at the transects AA′ shown in Figures 3b and 11a for (a) the steady state SS_c and (b) the transient state TS_1 together with (c) their autocorrelation functions, ACF. A smoother landscape at small scales, scales < approximately 7 mm or 50 mm^2, is observed during the *TS* both from the top plots (absence of large spikes [for example, a reduction of ∼30% in the number of large spikes, corresponding to a value of $\Delta h_x >$ 90th percentile at *SS*, was observed at *TS* at the location of transect AA′; see also, e.g., areas highlighted by the ellipse] and more consecutive same magnitude/sign elevation increments) and the ACF (increased autocorrelation and elimination of few distinct small scales at *SS*).

law exponent of ∼−1.1, while at the intermediate wavelengths (corresponding to approximately 6.5 mm–2.5 cm or 40–500 mm^2), the spectral slope is slightly greater than zero (slope of zero is a signature of white noise), suggesting spatially uncorrelated elevation increments and thus relatively rough landscape at those scales. The slope of the PSD for the increments observed here is in agreement with spectral slopes of natural landscape profiles which have been documented to be ∼−3 for elevations (∼−1 for elevation increments) [*Perron et al*., 2008]. Note that here we present wavelet spectra instead of Fourier spectra because wavelet filtering removes local nonstationarities in the signal. Also, the wavelet spectrum is smoother than the Fourier spectrum resulting in better distinction of the scaling regimes, and for signals with frequency/wave number content which evolves over time/space, it provides a better measure of the variance attributed to localized features of a given frequency compared to the Fourier spectrum [*Gamage and Blumen*, 1993; *Addison*, 2002; *Singh et al*., 2011]. We used the Mexican hat wavelet to compute the wavelet spectra in this study.

During climatic forcing (at the *TS*), scaling in the lower wave number regime does not vary, while at intermediate scales, it changes considerably. Within the intermediate scales, the energy reduction at smaller scales is higher than that at larger scales and this energy-reduction-interface shifts toward the lower wave numbers (larger scales) as the time proceeds. In fact, it can be seen that the debris-dominated regime shrinks as a function of time (Figure 13). We interpret this shrinking of regime as a redistribution of energy (variability) from smaller scales to intermediate and larger scales, i.e., the small scales force change in larger scales. This regime shrinking under the influence of changing climatic forcing can also be seen as reorganization of debris-dominated regime into a fluvial regime and is consistent with the observations that were made from the changing slope-area relationship from *SS* to *TS*. In other words, increasing precipitation results in a landscape with longer fluvial regime at the expense of shrinking the debris-dominated regime observed at the *SS*, suggesting an influence of smaller-scale features (higher wave number) on intermediate and larger scales as evident from Figure 13 and is consistent with the observations made from Figures 5, 11, and 12.

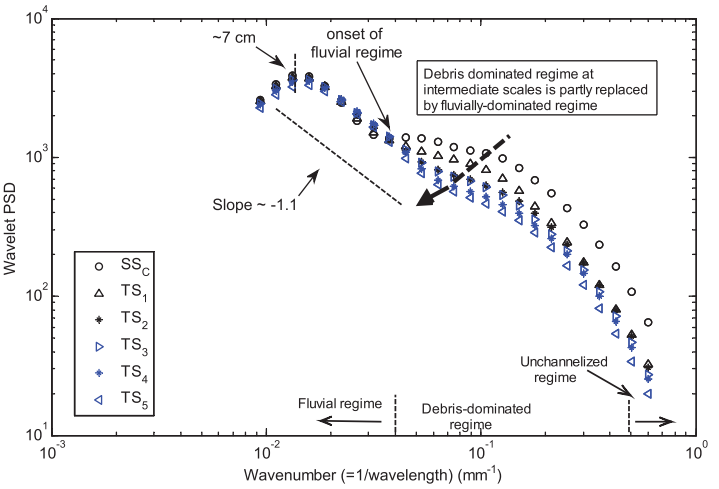

Figure 13. Wavelet power spectral density (PSD) of the spatial elevation increments of transect AA′ (see Figure 3b) as landscape evolves from steady state (SS_c) to the transient states (TS_i, $i=1, 2, 3, 4, 5$). The dotted arrow depicts the redistribution of energy (variability) within intermediate and larger scales consistent with the slope-area relationship which suggests an expansion of the fluvial regime from larger to intermediate scales during transient state.

6. Summary and Conclusions

Knowledge of the response of landscapes to changes in climate in terms of mean elevation change (macroscale) and reorganization of hillslopes, valleys, ridges, and channels (microscale) is an issue of interest in view of climatic trends in many regions of the world. Studies have shown that climatic change imprints distinct signatures on the evolving landscape. Understanding and quantifying these signatures of change is important as the underlying processes developing these landscapes exhibit complex dynamics and nonlinear behavior to the timing, frequency, and magnitude of the changing forcing, which needs to be understood for predicting landscape vulnerability to future climatic change. Since the time scale of these changes is very long, an attractive way to study this problem is via physical experiments where an experimental landscape is imposed to changing climatic forcing and its evolution studied in detail.

Although several studies have addressed the macro-scale response, studies that focus on the smaller-scale reorganization and the mechanistic progression of this change within different scales of the landscapes are lacking. One reason is the absence of data for such an analysis which requires very high-resolution spatio-temporal data of elevation fields which up until now was impossible to achieve. Such data were collected in the eXperimental Landscape Evolution (XLE) facility at the St. Anthony Falls Laboratory at the University of Minnesota. The data include measurements of high-resolution digital elevation models (DEMs) both in space (0.5 mm) and time (5 min) during the evolution of the landscape to achieve steady state *SS* (*SS* was achieved at approximately 8 h since initiation of the experiment), during a fivefold increase of precipitation for 30 min (transient state *TS*), and as the landscape started approaching a new steady state.

The main results of this study can be stated as follows.

1. With increasing precipitation, the slope-area relation changes considerably specifically for drainage basins corresponding to intermediate scales representing drainage areas of 2.5 mm^2 to around 250 mm^2. The change is more notable immediately following an increase in precipitation, than at later times, i.e., during the transient state (*TS*) of increased precipitation. Interpreting the slope-area relationship in terms of the physical mechanisms that resulted in landscape organization, we infer that increasing precipitation results in a landscape in which the fluvially dominated regime shifts from larger to progressively smaller scales at the expense of shrinking the debris-dominated (colluvial) regime observed in the steady state (*SS*) landscape (see Figure 5).
2. The probability distribution function (PDF) of elevation differences between two time instants within the *SS* and at the transition between *SS* and *TS* shows a shift toward positive elevation change (i.e., erosion) not only in the mean (as expected and consistent with the decreasing mean elevation of the landscape)

but also in the probability of exceedance of large erosional events (see Figure 6). This suggests a disproportional occurrence of large erosional events during transient state.

3. During *TS*, erosion is predominantly focused on the unchannelized parts of the landscape which results in smoothening of hillslopes, possibly rearrangement of the ridges of the low order basins, widening of valleys, and aggradation of channel beds. This is in contrast to the *SS* where notable erosion occurs in channels and close-by valleys. Several lines of evidence have been presented for these conclusions which include a correlation analysis of spatial elevation increments at *SS* and *TS*, an analysis of elevation map differences during transitional state, and an independent analysis of ~230 channel cross sections along several transects at steady and transient states.
4. The wavelet power spectral density (PSD) of the spatial elevation increments shows three distinct scaling regimes in agreement with the slope-area curve. During the *TS*, an increasing slope (in a log-log scale) for the intermediate scales compared to that at *SS* is observed. A steeper slope at intermediate scales in the PSD suggests a smoother topography (consistent with the correlation analysis) implying lower variability at the higher wave numbers (smaller scales) which is also consistent with the observation of a fluvial regime that expands by encroaching to smaller scales. We interpret the erosional acceleration during the *TS* which predominantly comes from the small-scale unchannelized parts of the landscape as the main mechanism that has forced changes at the intermediate to larger scales, specifically replacement of debris-dominated regime with fluvial regime.

In summary, we find that the landscape response to increased precipitation is rapid both in terms of sediment discharge and topographic adjustment at all scales. This rapid response is mainly driven by accelerated hillslope erosion which results in geometric adjustments of channel widths and hillslope angles. This leads to a reduction in larger local relief as ridgetops lower and to a lesser degree as channels infill with sediment. These results support past field-based findings by *Gabet et al*. [2004] and suggest that an exclusive focus on "fluvial landscape" response to climate change might be of limited utility [cf. *Whipple et al*., 1999; *Whipple and Tucker*, 1999; *Whittaker*, 2012].

Acknowledgments

This research was partially supported by the National Center for Earth-surface Dynamics (NCED), a Science and Technology Center funded by NSF under agreement EAR-0120914 and by NSF grant EAR-1209402 under the Water Sustainability and Climate Program. The senior author acknowledges the support of the Joseph T. and Rose S. Ling Endowed Professorship. We thank Jim Mullin and Chris Ellis as well as Michael Ellis and funding from the University of Exeter for helping us in developing the experimental facility (XLE). We thank Chris Paola for fruitful discussions. We also thank Ted Fuller, two anonymous reviewers, Editor, and Associate Editor, whose suggestions and constructive comments substantially improved our presentation and refined our interpretations. The data presented in this paper can be requested from the authors.

References

Abrahams, A. D., and A. J. Parsons (1991), Resistance to overland flow on desert pavements and its implications for sediment transport modeling, *Water Resour. Res.*, *27*(8), 1827–1836, doi:10.1029/91WR01010.

Abrahams, A. D., A. J. Parsons, and S. H. Luk (1986), Resistance to overland flow on desert hillslopes, *J. Hydrol.*, *88*, 343–363.

Addison, P. S. (2002), *The Illustrated Wavelet Transform Handbook*, 353 pp., Taylor and Francis, Philadelphia, Pa.

Baker, P. A., G. O. Seltzer, S. C. Fritz, R. B. Dunbar, M. J. Grove, P. M. Tapia, S. L. Cross, and H. D. Rowe (2001), The history of South American tropical precipitation for the past 25,000 years, *Science*, *291*, 640–643.

Bonnet, S. (2009), Shrinking and splitting of drainage basins in orogenic landscapes from the migration of the main drainage divide, *Nat. Geosci.*, *2*, 766–771, doi:10.1038/ngeo666.

Bonnet, S., and A. Crave (2003), Landscape response to climate change: Insights from experimental modeling and implications for tectonic versus climatic uplift of topography, *Geology*, *31*, 123–126.

Bonnet, S., and A. Crave (2006), Macroscale dynamics of experimental landscape, in *Analogue and Numerical Modelling of Crustal-Scale Processes, Geol. Soc. Spec. Publ.*, edited by S. J. H. Buiter and G. Schreurs, pp. 327–339, Geol. Soc., London, U. K.

Bookhagen, B., R. C. Thiede, and M. R. Strecker (2005), Late quaternary intensified monsoon phases control landscape evolution in the northwest Himalaya, *Geology*, *33*, 149–152.

Booth, A. M., J. J. Roering, and A. W. Rempel (2013), Topographic signatures and a general transport law for deep-seated landslides in a landscape evolution model, *J. Geophys. Res. Earth Surf.*, *118*, 603–624, doi:10.1002/jgrf.20051.

Brakenridge, G. R. (1980), Widespread episodes of stream erosion during the Holocene and their climatic cause, *Nature*, *283*, 655–656.

Brunsden, D. (1993), The persistence of landforms, *Z. Geomorphol. Suppl.*, *93*, 13–28.

Brunsden, D., and J. B. Thornes (1979), Landscape sensitivity and change, *Trans. Inst. Br. Geogr.*, *4*(4), 463–486.

Bull, W. B. (1991), *Geomorphic Responses to Climate Change*, pp. 326, Oxford Univ. Press, Oxford, U. K.

Burbank, D. W., J. Leland, E. Fielding, R. S. Anderson, N. Brozovic, M. R. Reid, and C. Duncan (1996), Bedrock incision, rock uplift and threshold hillslopes in the northwestern Himalayas, *Nature*, *379*, 505–510.

Burnett, A. P., M. J. Soreghan, C. A. Scholz, E. T. Brown (2011), Tropical East African climate change and its relation to global climate: A record from Lake Tanganyika, Tropical East Africa, over the past 90+ kyr, *Palaeogeogr. Palaeoclimatol. Palaeoecol.*, *303*, 155–167, doi: 10.1016/j.palaeo.2010.02.011.

D'Arcy, M., and A. C. Whittaker (2014), Geomorphic constraints on landscape sensitivity to climate in tectonically active areas, *Geomorphology*, *204*, 366–381.

Dietrich, W. E., D. Bellugi, L. S. Sklar, J. D. Stock, A. M. Heimsath, and J. J. Roering (2003), Geomorphic transport laws for predicting landscape form and dynamics, in *Prediction in Geomorphology, Geophys. Monogr. Ser.*, vol. 135, edited by P. Wilcock and R. Iverson, pp. 103–132, AGU, Washington, D. C.

Dietrich, W. E., and J. T. Perron (2006), The search for a topographic signature of life, *Nature*, *439*, 411–418, doi:10.1038/nature04452.

Fernandes, N. F., and W. E. Dietrich (1997), Hillslope evolution by diffusive processes: The timescale for equilibrium adjustments, *Water Resour. Res.*, *33*(6), 1307–1318, doi:10.1029/97WR00534.

Finnegan, N. J., R. Schumer, and S. Finnegan (2014), A signature of transience in bedrock river incision rates over timescales of 10^4-10^7 years, *Nature*, *505*(7483), 391–394, doi:10.1038/nature12913.
Foreman, B. Z., P. L. Heller and M. T. Clementz (2012), Fluvial response to abrupt global warming at the Palaeocene/Eocene boundary, *Nature*, *491*, 92–95.
Fuller, T. K., L. A. Perg, J. K. Willenbring, and K. Lepper (2009), Field evidence for climate-driven changes in sediment supply leading to strath terrace formation, *Geology*, *37*(5), 467–470, doi:10.1130/G25487A.1.
Gabet, E. J., B. A. Pratt-Sitaula, and D. W. Burbank (2004), Climatic controls on hillslope angle and relief in the Himalayas, *Geology*, *32*, 629–632.
Gamage, N. K. K., and W. Blumen (1993), Comparative analysis of low level cold fronts: Wavelet, Fourier, and empirical orthogonal function decompositions, *Mon. Weather Rev.*, *121*, 2867–2878.
Godard, V., G. E. Tucker, G. B. Fisher, D. W. Burbank, and B. Bookhagen (2013), Frequency-dependent landscape response to climatic forcing, *Geophys. Res. Lett.*, *40*, 859–863, doi:10.1002/grl.50253.
Goren, L., S. D. Willett, F. Herman, and J. Braun (2014), Coupled numerical-analytical approach to landscape evolution modeling, *Earth Surf. Processes Landforms*, *39*, 522–545, doi:10.1002/esp.3514.
Guala, M., A. Singh, N. BadHeartBull, and E. Foufoula-Georgiou (2014), Spectral description of migrating bed forms and sediment transport, *J. Geophys. Res. Earth Surf.*, *119*, 123–137, doi:10.1002/2013JF002759.
Hack, J. T. (1960), Interpretation of erosional topography in humid temperate regions, *Am. J. Sci.*, *258A*, 80–97.
Hancock, G. (1997), Experimental testing of the Siberia landscape evolution model, PhD thesis, 467 pp., Univ. of Newcastle, Newcastle, N. S. W., Australia.
Hancock, G., and Willgoose, G. (2001a), The production of digital elevation models for experimental model landscapes, *Earth Surf. Processes Landforms*, *26*, 475–490, doi:10.1002/esp.187.
Hancock, G., and G. Willgoose (2001b), Use of a landscape simulator in the validation of the SIBERIA Catchment Evolution Model: Declining equilibrium landforms, *Water Resour. Res.*, *37*(7), 1981–1992, doi:10.1029/2001WR900002.
Hartshorn, K., N. Hovius, W. B. Dade, and R. L. Slingerland (2002), Climate-drive bedrock incision in an active mountain belt, *Science*, *297*, 2036–2038.
Hasbargen, L., and C. Paola (2003), How predictable is local erosion rate in erosional landscapes? in *Prediction in Geomorphology, Geophys. Monogr. Ser.*, vol. 136, edited by P. R. Wilcock, and R. M. Iverson, pp. 231–240, AGU, Washington, D. C.
Hasbargen, L. E., and C. Paola (2000), Landscape instability in an experimental drainage basin, *Geology*, *28*, 1067–1070.
Intergovernmental Panel on Climate Change (2007), Climate change 2007: The physical science basis, in *Contribution of Working Group I to the Fourth Assessment Report of the Intergovernmental Panel on Climate Change*, edited by S. Solomon et al., Cambridge Univ. Press, Cambridge, U. K.
Jerolmack, D. J., and C. Paola (2010), Shredding of environmental signals by sediment transport, *Geophys. Res. Lett.*, *37*, L19401, doi:10.1029/2010GL044638.
Keylock, C. J., A. Singh, and E. Foufoula-Georgiou (2014), The complexity of gravel bed river topography examined with gradual wavelet reconstruction, *J. Geophys. Res. Earth Surf.*, *119*, 682–700, doi:10.1002/2013JF002999.
Knox, J. C. (1983), Responses of river systems to Holocene climates, in *Late Quaternary Environments of the United States, vol. 2, The Holocene*, edited by H. E. Wright and S. C. Porter, pp. 26–41, Univ. of Minn. Press, Minneapolis.
Lague, D. (2014), The stream power river incision model: Evidence, theory and beyond, *Earth Surf. Processes Landforms*, *39*(1), 38–61.
Lague, D., and P. Davy (2003), Constraints on the long-term colluvial erosion law by analyzing slope-area relationships at various tectonic uplift rates in the Siwaliks Hills (Nepal), *J. Geophys. Res.*, *108*(B2), 2129, doi:10.1029/2002JB001893.
Lague, D., A. Crave, and P. Davy (2003), Laboratory experiments simulating the geomorphic response to tectonic uplift, *J. Geophys. Res.*, *108*(B1), 2008, doi:10.1029/2002JB001785.
Lavé, J., and J. P. Avouac (2000), Active folding of fluvial terraces across the Siwaliks Hills, Himalayas of central Nepal, *J. Geophys. Res.*, *105*(B3), 5735–5770, doi:10.1029/1999JB900292.
Meyer, G. A., S. G. Wells, R. C. Balling Jr., and A. J. T. Jull (1992), Response of alluvial systems to fire and climate change in Yellowstone National Park, *Nature*, *357*, 147–150.
Michaelides, K., and M. B. Singer (2014), Impact of coarse sediment supply from hillslopes to the channel in runoff-dominated, dryland fluvial systems, *J. Geophys. Res. Earth Surf.*, *119*, 1205–1221, doi:10.1002/2013JF002959.
Milly, P. C. D., R. T. Wetherald, T. L. Delworth, and K. A. Dunne (2002), Increasing risk of great floods in a changing climate, *Nature*, *415*, 514–517.
Molnar, P. (2001), Climate change, flooding in arid environments, and erosion rates, *Geology*, *29*, 12, 1071.
Montgomery, D. R. (2001), Slope distributions, threshold hillslopes, and steady-state topography, *Am. J. Sci.*, *301*, 432–454.
Montgomery, D. R., and E. Foufoula-Georgiou (1993), Channel network source representation using digital elevation models, *Water Resour. Res.*, *29*(12), 3925–3934, doi:10.1029/93WR02463.
Montgomery, D. R., G. Balco, and S. D., Willett (2001), Climate, tectonics, and the morphology of the Andes, *Geology*, *29*, 579–582.
National Research Council (2010), *Landscapes on the Edge: New Horizons for Research on Earth's Surface*, 180 pp., Natl. Acad. Press, Washington, D. C.
Paola, C., K. Straub, D. Mohrig, and L. Reinhardt (2009), The "unreasonable effectiveness" of stratigraphic and geomorphic experiments, *Earth Sci. Rev.*, *97*, 1–43.
Parker, R. S. (1977), Experimental study of basin evolution and its hydrologic implications, PhD dissertation, Colo. State Univ., Fort Collins, Colo.
Passalacqua, P., F. Port-Agel, E. Foufoula-Georgiou, and C. Paola (2006), Application of dynamic subgrid-scale concepts from large-eddy simulation to modeling landscape evolution, *Water Resour. Res.*, *42*, W06D11, doi:10.1029/2006WR004879.
Pelletier, J. D. (1999), The self-organization and scaling relationships of evolving river networks, *J. Geophys. Res.*, *104*(B4), 7359–7375, doi:10.1029/1998JB900110.
Pelletier, J. D., B. D. Malamud, T. A. Blodgett, and D. L. Turcotte (1997), Scale-invariance of soil moisture variability and its implications for the frequency-size distribution of landslides, *Eng. Geol.*, *48*, 254–268.
Perron, J. T., J. W. Kirchner, and W. E. Dietrich (2008), Spectral signatures of characteristic spatial scales and nonfractal structure in landscapes, *J. Geophys. Res.*, *113*, F04003, doi:10.1029/2007JF000866.
Reinhardt, L., and M. A. Ellis (2015), The emergence of topographic steady-state in a perpetually dynamic self-organized critical landscape, *Water Resour. Res.*, doi:10.1002/2014WR016223, in press.

Reinhardt, L., D. J. Jerolmack, B. J. Cardinale, V. Vanacker, and J. Wright (2010), Dynamic interactions of life and its landscape: Feedbacks at the interface of geomorphology and ecology, *Earth Surf. Processes Landforms*, *35*, 78–101.

Rigon, R., A. Rinaldo, and I. Rodríguez-Iturbe (1994), On landscape self-organization, *J. Geophys. Res.*, *99*(B6), 11,971–11,993, doi:10.1029/93JB03601.

Rigon, R., I. Rodríguez-Iturbe, A. Rinaldo, A. Giacometti, A. Maritan, D. Tarboton, and A. Rinaldo (1996), On Hack's law, *Water Resour. Res.*, *32*(11), 3367–3374, doi:10.1029/96WR02397.

Rinaldo, A., I. Rodríguez-Iturbe, R. L. Bras, and E. Ijjász-Vásquez (1993), Self-organized fractal river networks, *Phys. Rev. Lett.*, *70*, 822–826.

Rinaldo, A., W. E. Dietrich, R. Rigon, G. Vogel, and I. Rodríguez-Iturbe (1995), Geomorphological signatures of varying climate, *Nature*, *374*, 632–634.

Rodríguez-Iturbe, I., E. J. Ijjász-Vásquez, R. L. Bras, and D. G. Tarboton (1992), Power law distributions of discharge mass and energy in river basins, *Water Resour. Res.*, *28*(4), 1089–1093, doi:10.1029/91WR03033.

Sapozhnikov, V. B., and E. Foufoula-Georgiou (1997), Experimental evidence of dynamic scaling and indications of self-organized criticality in braided rivers, *Water Res. Res.*, *33*(8), 1983–1991, doi:10.1029/97WR01233.

Schumm, S. A., M. P. Mosley, and W. E. Weaver (1987), *Experimental Fluvial Geomorphology*, 413 pp., John Wiley, N. Y.

Sklar, L., and W. E. Dietrich (1998), River longitudinal profiles and bedrock incision models: Stream power and the influence of sediment supply, in *Rivers Over Rock: Fluvial Processes in Bedrock Channels, Geosphys. Monogr. Ser.*, edited by K. J. Tinkler and E. E. Wohl, pp. 237–260, AGU, Washington, D. C.

Slater, L. J., and M. B. Singer (2013), Imprint of climate and climate change in alluvial riverbeds: Continental United States, 1950–2011, *Geology*, *41*(5), 595–598.

Singh, A., F. Porté-Agel, and E. Foufoula-Georgiou (2010), On the influence of gravel bed dynamics on velocity power spectra, *Water Resour. Res.*, *46*, W04509, doi:10.1029/2009WR008190.

Singh, A., S. Lanzoni, P. R. Wilcock, and E. Foufoula-Georgiou (2011), Multi-scale statistical characterization of migrating bedforms in gravel and sand bed rivers, *Water Resour. Res.*, *47*, W12526, doi:10.1029/2010WR010122.

Smith, B. J. (1982), Effects of climate and land-use change on gully development: An example from northern Nigeria, *Z. Geomorphol. Suppl.*, *44*, 33–51.

Tarboton, D. G. (1997), A new method for the determination of flow directions and upslope areas in grid digital elevation models, *Water Resour. Res.*, *33*(2), 309–319, doi:10.1029/96WR03137.

Tucker, G. E., and R. L. Bras (1998), Hillslope processes, drainage density, and landscape morphology, *Water Resour. Res.*, *34*(10), 2751–2764, doi:10.1029/98WR01474.

Tucker, G. E., and G. R. Hancock (2010), Modelling landscape evolution, *Earth Surf. Processes Landforms*, *35*, 28–50. doi:10.1002/esp.1952.

Tucker, G. E., and R. Slingerland (1997), Drainage basin responses to climate change, *Water Resour. Res.*, *33*(8), 2031–2047, doi:10.1029/97WR00409.

Turowski, J. M., A. Badoux, J. Leuzinger, and Ramon Hegglin (2013), Large floods, alluvial overprint, and bedrock erosion, *Earth Surf. Processes Landforms*, *38*, 947–958.

Whipple, K. X., and G. E. Tucker (1999), Dynamics of the stream-power river incision model: Implications for height limits of mountain ranges, landscape response timescales, and research needs, *J. Geophys. Res.*, *104*(B8), 17,661–17,674, doi:10.1029/1999JB900120.

Whipple, K. X., E. Kirby, and S. H. Brocklehurst (1999), Geomorphic limits to climate-induced increases in topographic relief, *Nature*, *401*, 39–43.

Whittaker, A. C. (2012), How do landscapes record tectonics and climate?, *Lithosphere*, *4*(2), 160–164, doi:10.1130/rf.l003.1.

Willgoose, G. (1994), A statistic for testing the elevation characteristics of landscape simulation models, *J. Geophys. Res.*, *99*(B7), 13,987–13,996, doi:10.1029/94JB00123.

Willgoose, G. R., R. L. Bras, and I. Rodriguez-Iturbe (1991), Results from a new model of river basin evolution, *Earth Surf. Processes Landforms*, *16*, 237–254.

Zaprowski, B. J., F. J. Pazzaglia, and E. B. Evenson (2005), Climatic influences on profile concavity and river incision, *J. Geophys. Res.*, *110*, F03004, doi:10.1029/2004JF000138.